HOLE EXTENSION EFFECT ON TRANSPIRATION FLOW EFFICIENCY

TOMASZ LEWANDOWSKI AND PIOTR DOERFFER

Institute of Fluid Flow Machinery, Polish Academy of Sciences
Fiszera 14, 80-952, Gdansk, Poland

(received: 15 January 2015; revised: 16 February 2015;
accepted: 20 February 2015; published online: 25 March 2015)

Abstract: The present analysis of the hole extension effect on the transpiration flow efficiency is a part of the research [1] which aims at defining a physical transpiration model of the flow through perforated plates. Perforated walls find a wide use as a method of flow control and effusive cooling. Some data on the L/D (hole length to diameter ratio) effect on the flow structure and mass flow rate may be found in the literature [2, 3], but all those works concern holes of a diameter at least one order of magnitude larger than those used in the simulations presented in this paper. Due to the size of the analyzed holes and their cylindrical shape, the only method of analysing the flow through such holes is the numerical method. In the conducted simulations, the holes were $D = 0.6$ mm, 0.3 mm and 0.125 mm in diameter and the perforation values were equal to 4%, 5%, 8% and 10%. The L/D ratio was changed between 0.25 and 8. The data bank of the flow through the cylindrical holes was produced. The hole extension has a significant influence on the obtained mass flow rate and, consequently, on the transpiration flow efficiency. In addition, entrance effects appear to be important.

Keywords: perforated wall, L/D ratio, mass flow rate, efficiency

Nomenclature

D – hole diameter (m)
L – hole length (m)
Ma – Mach number
P – pressure (Pa)
Re – Reynolds number
S – perforation (%)
U – velocity ($\mathrm{m{\cdot}s^{-1}}$)
h – enthalpy (J)
$\dot{m}$ – mass flow rate
η – efficiency

Indexes:

0 – stagnation conditions, inlet

2 – outlet
geo – geometrical
is – isentropic

1. Introduction

The influence of the hole extension (the length to diameter ratio) on the perforated plate efficiency is analyzed in the literature, mainly in articles about film cooling of gas turbine blades. It has been extensively studied in many experiments [2, 3] and numerical simulations [4]. These articles focus primarily on changes of the thermal efficiency of film cooling at the hole exit, while the behaviour of the fluid inside the hole has not been analysed in detail. The authors [2, 3] have focused on the problem how changes of the L/D ratio affect the behaviour of the main flow. The L/D ratio has been changed within the range from 0.5 to 12. The present article examines, based on CFD simulations, the influence of the hole extension on the perforated plate flow efficiency and structure. Due to the size of the analyzed holes and their cylindrical shape, the only method of analysing the flow through such holes is the numerical method. Various ranges of pressure differences were investigated. The studies were performed for various Mach numbers up to the critical conditions (chocking flow in the holes). The assumed L/D ratio values were within the range similar to that found in the literature, but in our cases the holes had a diameter several times smaller than the smallest value analyzed in the literature. The presented analysis is purely numerical, but ref. [1] testifies the good coincidence of simulation results with experimental data [5, 6] within the examined pressure ranges.

2. Research scope and numerical model

The 3D steady-state flow through perforated plates was simulated using the ANSYS/FLUENT commercial code. The pressure-velocity coupling was done using the SIMPLE algorithm. Spatial derivatives were approximated using a second order upwind scheme. The simulated space was restricted to a single hole in the perforated plate. Figure 1 presents the simulation domain consisting of 0.55–0.9 million mesh cells, depending on the hole length. The mesh resolution near the solid wall boundaries was assumed in such a way that y_+ was below 1. In the middle part, a cylindrical hole can be seen between the inlet and outlet zones of the hexagonal cross section. The total pressure at the inlet and static pressure at the outlet boundary conditions were applied. Symmetry boundaries were applied as the side boundaries of the inlet and outlet zones, because the direction of the flow and the hole was perpendicular to that of the perforated plate surface. This approach enables modeling the flow through perforated plate with infinite number of holes. The size of the hexagonal surface depends on the assumed geometrical perforation S_{geo} and hole diameter D.

In the reported simulations, the holes were $D = 0.6\,\mathrm{mm}$, $0.3\,\mathrm{mm}$ and $0.125\,\mathrm{mm}$ in diameter. The wall thickness was from $L = 0.03125\,\mathrm{mm}$ to $L = 4.8\,\mathrm{mm}$,

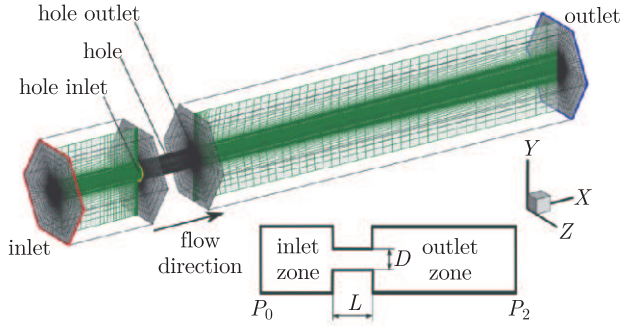

Figure 1. Computational domain, grid and cross section

which corresponded to the L/D ratio range between 0.25 and 8. The perforation values were equal to 4%, 5%, 8% and 10%. Mass flow rate changes were obtained by changing the outlet pressure. Changes of pressure drop $\Delta P/P_0$ ranged from 0.06 to 0.6. All the performed simulations covered the Reynolds number range from 500 to 15 000. Previous simulations [1] have demonstrated that mass flow rate differences between laminar and turbulent flow cases amount only to about 1%, therefore now the turbulent flow model was used for all flow cases. The one-equation Spalart-Allmaras turbulence model was selected due to its better calculation convergence and the obtained symmetry in the flow structure [1].

3. Effect of hole elongation on the flow structure

The database of numerical results contains a large number of the examined cases, varying by perforation values, hole diameters, channel lengths and pressure drops. The effect of the elongation on the flow structure is demonstrated based on the critical test case. The critical case means the critical pressure drop over the perforated plate ($P_0 = 10\,1325$ Pa, $P_2 = 40\,246$ Pa). The geometrical perforation for that case is equal to $S_{\text{geo}} = 4\%$. The Mach number contour plots in the longitudinal cross-section of the simulation space for the critical case and three diameters are presented in Figure 2.

The contours for the same diameter were made in the same color scale of the Mach number in order to better visualize the flow structure. For diameter $D = 0.6$ mm it was 0 to 1.77, for $D = 0.3$ mm it was 0 to 1.59 and $D = 0.125$ mm it was 0 to 1.53. One can see that reducing the diameter leads to decreasing the maximum Mach number. In all cases, there is flow acceleration at the hole inlet. It is associated with the change of the open area for the flow – sudden flow contraction. It can be noted that for the largest L/D the flow inside the channel is the slowest. As L/D decreases, the flow structure through the channel becomes more complex. An additional insight into the structure of the flow in the hole can be obtained based on the Mach number distribution along the channel axis. Figure 3 presents the Mach number Ma as a function of the normalized length of the channel x/L along the center line of the hole. For diameters $D = 0.6$ mm (Re = 3200) and $D = 0.3$ mm (Re = 6500) and for $L/D > 1$ the flow in the channel

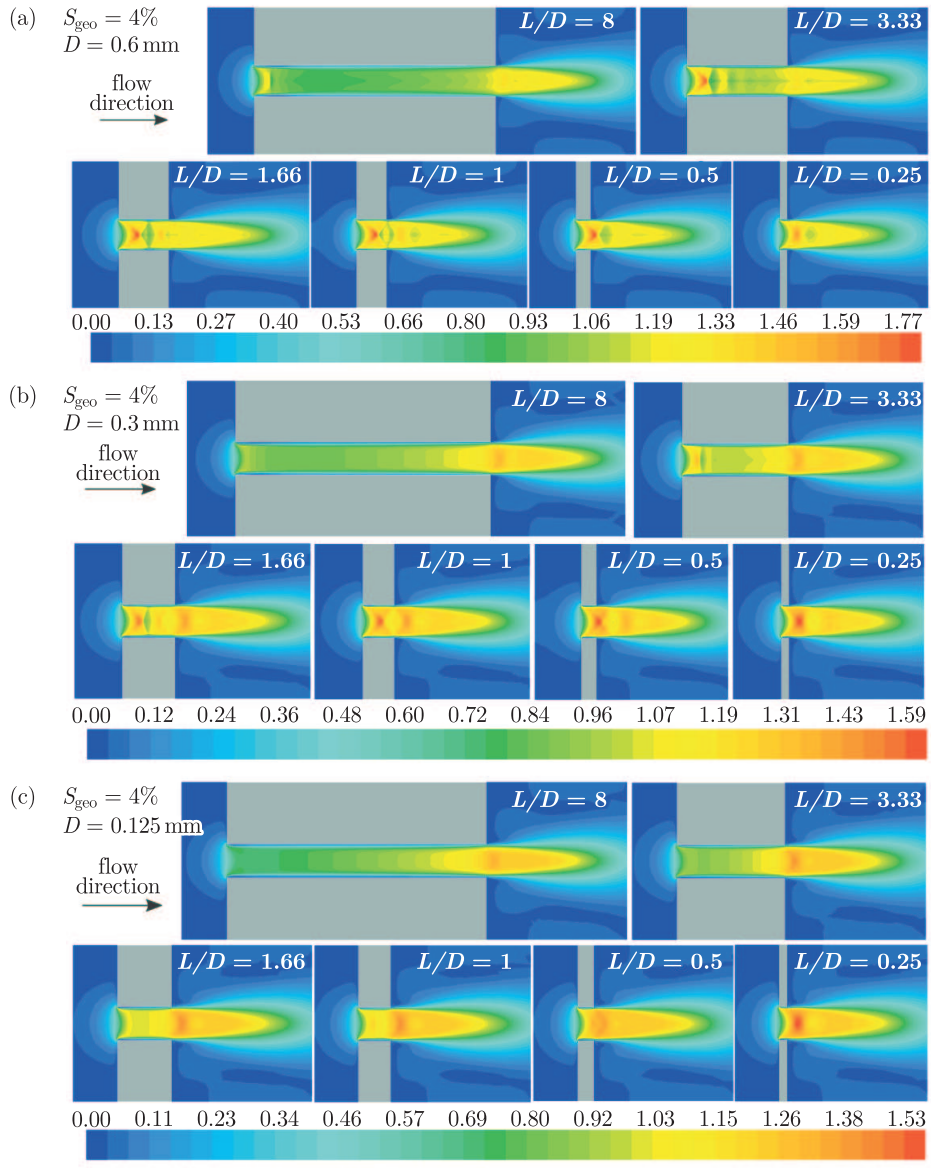

Figure 2. Mach number in the channel for diameters: (a) $D = 0.6\,\text{mm}$, (b) $D = 0.3\,\text{mm}$ and (c) $D = 0.125\,\text{mm}$

alternately speeds up and slows down. The inlet expansion is the smallest for the longest channel. The maximum inlet expansion is for L/D equal 1.6 and 1. Generally, for L/D less than unity the maximum velocity occurs outside of the channel and the acceleration takes place through the entire channel length. For these cases, all variations of the flow structure are situated outside the duct. The flow characteristics for diameter $D = 0.3\,\text{mm}$ behave very similarly to those recorded for the diameter $D = 0.6\,\text{mm}$.

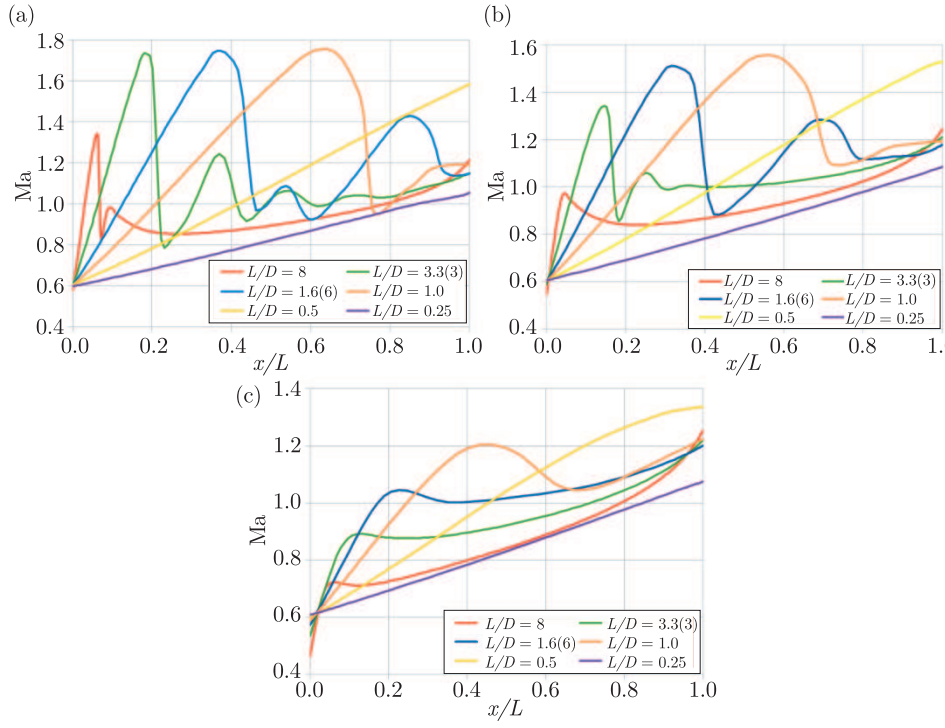

Figure 3. Mach number vs. normalized channel length x/L along the center line for diameters: (a)$D = 0.6\,\text{mm}$, (b) $D = 0.3\,\text{mm}$ and (c)$D = 0.125\,\text{mm}$

A slightly different distribution of the Mach number along the axis was obtained for the hole of diameter $D = 0.125\,\text{mm}$ and $L/D > 1$. For this diameter the flow accelerates over the entire length of the channel without any significant fluctuation. The maximum acceleration takes place outside the channel. Figure 4 presents the Mach number along the axis of the channel extended by two diameters outside, for diameter $D = 0.6\,\text{mm}$ and different L/D values.

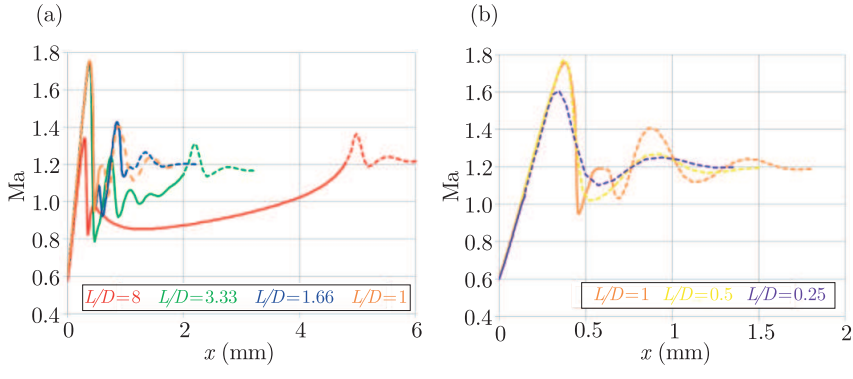

Figure 4. Mach number vs. channel axis length extended by two diameters outside: $D = 0.6\,\text{mm}$ and different L/D values: (a) $L/D \geq 1$, (b) $L/D \leq 1$

The solid lines represent the Mach number in the channel and the dotted lines represent the Mach number along the axis but outside the channel. For the same diameter, the Mach number gradient at the entrance to the channel is the same, even for the smallest L/D values, where the maximum Mach number appears outside the channel. As compared to larger diameters, the inlet expansion for $D = 0.125\,\text{mm}$ is lower and its region is shorter, see Figure 5.

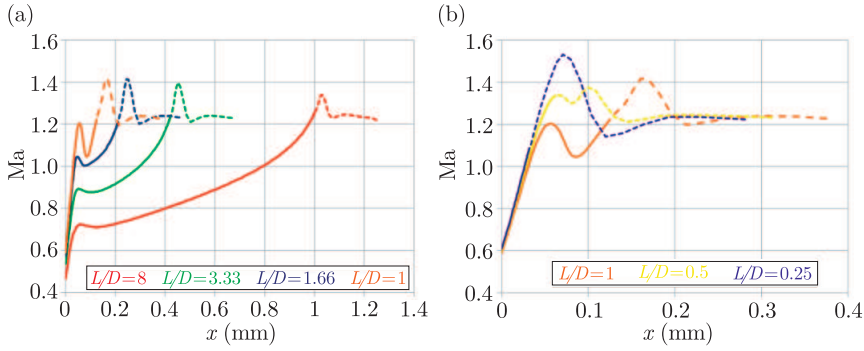

Figure 5. Mach number vs. channel axis length extended by two diameters outside: $D = 0.125\,\text{mm}$ and different L/D value: (a) $L/D \geq 1$, (b) $L/D \leq 1$

The presented comparison shows that the hole length affects the flow expansion at the inlet. The longer the channel, the smaller the inlet expansion. One can see that for the same pressure drop, when L/D decreases the structure of the flow becomes more complex. However, this conclusion does not refer to the channel with the smallest hole diameter.

4. Effect of L/D on the mass flow rate and efficiency

Figure 6 shows the influence of L/D on the mass flow rate for three different pressure drops. Symbols from Figure 6 are explained in the Table 1.

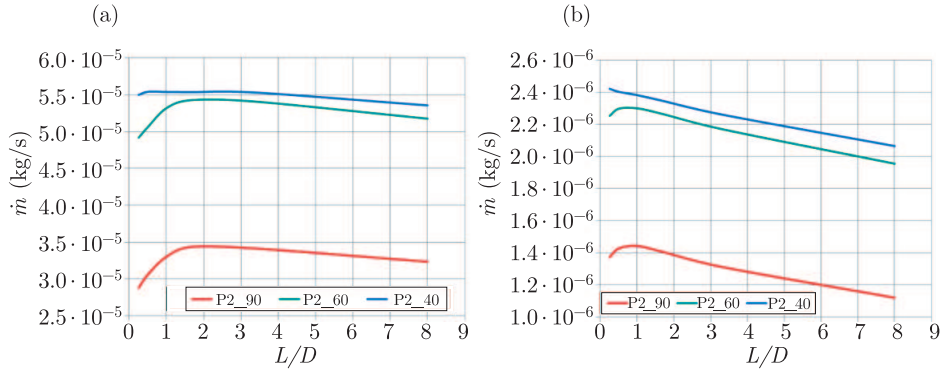

Figure 6. Mass flow rate for different L/D, three different pressure drops, and channel diameter: (a) $D = 0.6\,\text{mm}$, (b) $D = 0.125\,\text{mm}$

Table 1. Description of symbols

Symbol	P_0 (Pa)	P_2 (Pa)
P2_40	101 325	40 246
P2_60	101 325	60 246
P2_90	101 325	90 246

The characteristics of the mass flow rate for the diameter $D = 0.3$ mm are similar to those for the diameter $D = 0.6$ mm. Therefore, only the results for diameters $D = 0.6$ mm and 0.125 mm are shown.

For the cases below of the critical pressure drop (red and green lines), the maximum mass flow rate occurs for the smaller L/D value and the smaller diameter. For diameter $D = 0.6$ mm and critical pressure drop (blue line) the maximum mass flow rate shifts towards lower L/D values, as compared to the lower pressure drop. For the critical pressure drop value, the maximum value of mass flow rate appears at the L/D below one for all diameters. In our simulations the mass flow rate magnitude is directly related to the flow efficiency.

The efficiency of the transpiration flow is an effective feature which characterizes the perforated plate. In the real flow with losses the efficiency can be expressed using enthalpy $\left(\eta = (h_0 - h_2)/(h_0 - h_{is})\right)$ leading to the velocity ratio $\eta = U_2/U_{is}$. In another approach, used in this paper, the efficiency is defined by the stagnation pressure loss:

$$\eta = \frac{P_{02} - P_2}{P_0 - P_2} \tag{1}$$

where P_{02} represents the stagnation pressure at the hole outlet. Relation (1) expresses the loss in the stagnation pressure across the perforated plate. The plate efficiency can be determined individually for a single set of properties (pressure drop, hole length, diameter). It is more useful however to determine one efficiency value for the plate in the entire pressure range. The calculated efficiency is plotted in Figure 7 for $S_{geo} = 4\%$. It can be noticed that for $L/D = 1$ the efficiency values are similar for different diameters – Figure 7a. This case corresponds to the orange curves in Figure 3 and flow structure ($L/D = 1$) in Figure 2.

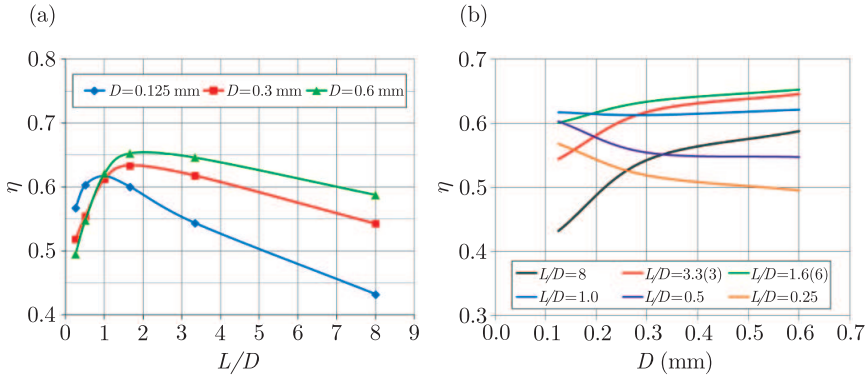

Figure 7. Changes of efficiency η for: (a) L/D ($S_{geo} = 4\%$), (b) diameter D ($S_{geo} = 4\%$)

Extending the channel ($L/D > 1$) leads to higher flow losses caused by friction and lower efficiency. For this L/D range the linear relation was obtained. Figure 7b presents the dependence of η on the hole diameter. The curves represent constant L/D values. For $L/D > 1$ the increase in diameter leads to an increase in efficiency, while for $L/D < 1$ the trend is opposite. For the range $L/D < 1$ the efficiency drop is caused by the „Vena Contracta" effect, which reduces the effective hole diameter.

5. Conclusions

The presented analysis enables better understanding of the phenomena occurring in the holes of a perforated plate. For larger holes (diameters 0.6 mm and 0.3 mm, Re from 3000 to 7000), a decrease in L/D leads to a more complex structure of the flow inside the hole. The axial velocity fluctuates along the hole length, speeds up and slows down alternately.

The inlet expansion depends on the channel length and also on the hole diameter. For small diameter holes (0.125 mm) there are no velocity peaks of the flow at the inlet (except $L/D = 1$) and the uniform flow develops until the hole outlet, displaying uniform acceleration along the entire hole. The maximum mass flow rate occurs for different L/D values for different diameters. For the same diameter and different pressure drops (below critical) the maximum mass flow rate for the same L/D value was obtained. For small diameter holes and the critical pressure drop (P2_40) the maximum mass flow rate occurs for very small L/D values, out of the analyzed range.

The mass flow rate characteristics have significant influence on the obtained efficiency values. For large diameters, the efficiency characteristics exhibit similar behavior like the mass flow rate in relation to the L/D values. The maximum efficiency value occurs for the same L/D ratio like the maximum mass flow rate. For $L/D = 1$ the efficiency values are similar for different diameters.

Acknowledgements

This research was supported by CI TASK and in part by PL-Grid Infrastructure.

References

[1] Lewandowski T and Doerffer P 2012 *Aerosp. Sci. Technology* **22** (1) 58
[2] Lutum E and Johnson B V 1999 *Turbomachinery J.* **121** 209
[3] Wilfert G and Wolff S 2001 *Turbomachinery J.* **122** 327
[4] Cerri G, Giovannelli A, Battisti L and Fedrizzi R 2007 *Appl. Thermal Eng.* **27** 692
[5] Doerffer P and Bohning R 2000 *Aerosp. Sci. Technol.* **4** (8) 524
[6] Doerffer P and Bohning R 2003 *Aerosp. Sci. Technol.* **7** (3) 171